

# Manifolds of exceptional points and effective Zeno limit of an open two-qubit system

Vladislav Popkov,<sup>1,2</sup> Carlo Presilla,<sup>3,4</sup> and Mario Salerno<sup>5</sup>

<sup>1</sup>Faculty of Mathematics and Physics, University of Ljubljana, Jadranska 19, SI-1000 Ljubljana, Slovenia

<sup>2</sup>Bergisches Universität Wuppertal, Gauss Str. 20, D-42097 Wuppertal, Germany

<sup>3</sup>Dipartimento di Matematica, Sapienza Università di Roma, Piazzale A. Moro 2, 00185 Rome, Italy

<sup>4</sup>Istituto Nazionale di Fisica Nucleare, Sezione di Roma 1, 00185 Rome, Italy

<sup>5</sup>Dipartimento di Fisica "E.R. Caianiello", Università di Salerno,

Via Giovanni Paolo II, 84084 Fisciano (SA), Italy

(Dated: December 19, 2024)

We analytically study the exceptional points of a Liouvillian super-operator describing an open quantum system of two interacting qubits with a dissipative bath of polarization applied to one of the qubits. Our focus is the structure of the exceptional point manifolds in the parameter space which we describe in all analytic details. In particular, we characterize the manifold of bifurcation points corresponding to largest dissipation, and describe the relative effective quantum Zeno dynamics in the bifurcation-free regime, which may occur at relatively small dissipation.

*Introduction.*—Strong spectral response to perturbations occurs in open quantum systems at their branch-point singularities, the so-called exceptional points (EPs) [1–3]. This phenomenon can be used for sensing [4, 5], hardware encryption [6], optimizing performance of quantum thermal machines [7], realizing a multipoint switch between modes in photonic systems [8], and other applications [9].

In classical and semiclassical systems in which quantum jumps are ignored, EPs are usually associated to degeneracies of non-Hermitian Hamiltonians and in this context several theoretical aspects of EPs are now well understood. At quantum level, an important class of systems where EPs appear is represented by the so called Markovian open systems, also known as quantum dynamical semigroups, whose time evolution obeys a Lindblad master equation according to which the generator of the quantum dynamical semigroup is a time-independent Liouvillian super-operator [10–12]. For these systems, we may have exceptional points of the Liouvillian (LEPs), i.e., points in the parameter space where the eigenvalues and eigenvectors of the Liouvillian superoperator coalesce (or, split, depending on the direction of variation of the parameters).

In contrast to the EPs of non-Hermitian Hamiltonians, the LEPs include quantum jumps that reflect the open nature of the systems and allow a comprehensive understanding of their dynamics in interaction with the environment [13]. Moreover, LEPs provide informations that are crucial in the analysis of rapidly decaying states in systems subject to decoherence [14].

The distribution of LEPs induced by the interplay between non-Hermitian dynamics and dissipation gives rise to Liouvillian exceptional point manifolds (LEPMs) in the parameter space. The knowledge of these manifolds is required for managing the system, for example, to optimize sensing applications close to LEPs with respect to system parameters. Operating in the complementary regions of LEPMs (i.e., in the regions where LEPs can-

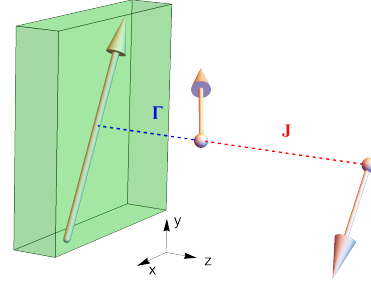


FIG. 1. An open two-qubit system is schematized as two  $XYZ$  Heisenberg spins  $1/2$  interacting via anisotropic exchange energies of strength  $J \equiv (J_x, J_y, J_z)$ . The system is coupled to a polarization dissipative bath (green box with a large arrow inside) only through one of the two spins. The red and blue dashed lines represent the Heisenberg exchange interaction between the two spins and the coupling  $\Gamma$  between the first spin and the bath, respectively. Small spheres indicate the sites on which the spins are located.

not occur) may be critical to optimize applications for which it is important to avoid instabilities, such as in the case of quantum computing. Moreover, the knowledge of LEPMs permits to delimit regions in the parameter space where the transition to the Zeno regime could be achieved with the lowest possible dissipative coupling to the environment.

Except for a few solvable cases involving two [15] and three-level systems [16], LEPMs, to our knowledge, are practically unexplored [17] (we discard all cases for which LEPs reduce to EPs of non Hermitian Hamiltonians as for example in [17]).

The aim of the present manuscript is to provide a full analytical characterization of all the LEPMs of a two-qubit system and to show how LEPMs can be used to optimize the phase transitions of the system to an effective Zeno regime by keeping the dissipative couplings with the environment as small as possible. In particular,

we consider two  $XYZ$  Heisenberg spins  $1/2$  interacting with exchange anisotropies  $J \equiv (J_x, J_y, J_z)$  and coupled to a dissipative polarization bath through one of the two spins only (see Fig. 1). The parameter space is tridimensional and consists, without loss of generality, of the two parameters,  $\gamma = J_y/J_x, \Delta = J_z/J_x$  (with  $J_x$  fixed to 1), for the Hamiltonian and one parameter,  $\Gamma$ , fixing the strength of the dissipative coupling to the bath. We take advantage of a  $Z_2$  symmetry to block-diagonalize the Liouvillian super-operator into two blocks, one of which is independent of  $\Delta$ . Using this symmetry, we derive polynomial equations that describe all the LEPs. We show that, by restricting only to real values of the parameters, for the  $\Delta$ -independent block, LEPs reduce to two planes,  $\Gamma = 8$  and  $\Gamma = 8\gamma$ , while for the other block, they exhibit more intricate topologies with a number of sheets (branches) varying between 1 and 6, depending on parameter values. Quite remarkably, from the intersection curves of some of these surfaces it is possible to derive a phase diagram in the  $\gamma - \Delta$  plane for effective Zeno transitions occurring at small dissipation. We show that these results are in good agreement with a perturbative calculation that extrapolates the strong Zeno regime to small dissipations.

*Two qubit model and Liouvillian symmetry.*—We consider an open system of two qubits undergoing an anisotropic exchange interaction of strength  $(1, \gamma, \Delta)$  in the  $(x, y, z)$  directions, respectively, and a Markovian dissipation of strength  $\Gamma$  acting only on qubit 1. The reduced density matrix  $\rho$  of the system evolves in time according to the Lindblad master equation

$$\frac{\partial \rho}{\partial t} = \mathcal{L}\rho, \quad (1)$$

where

$$\mathcal{L}\rho = -i[H, \rho] + \Gamma (L\rho L^\dagger - \frac{1}{2}(L^\dagger L\rho + \rho L^\dagger L)), \quad (2)$$

with jump operator  $L = \sigma^+ \otimes I_2$ ,  $I_n$  being the  $n \times n$  identity matrix, and Hamiltonian

$$H = \sigma^x \otimes \sigma^x + \gamma \sigma^y \otimes \sigma^y + \Delta \sigma^z \otimes \sigma^z. \quad (3)$$

As usual,  $\sigma^\pm = (\sigma^x \pm i\sigma^y)/2$ , with  $\sigma^x, \sigma^y, \sigma^z$  being the Pauli matrices. We work in units of  $\hbar = 1$  and Heisenberg anisotropy in the  $x$  direction  $J_x = 1$ , i.e.,  $t = t_{ph}J_x/\hbar$  and  $\Gamma = \Gamma_{ph}\hbar/J_x$ , where  $t_{ph}$  and  $\Gamma_{ph}$  are the physical time and the physical dissipation strength obtained for the effective values of  $\hbar$  and  $J_x$ . In present units the parameters  $\gamma, \Delta, \Gamma$  as well as the time  $t$  and the operators  $H$  and  $\mathcal{L}$  are dimensionless. Note also that  $H = H(\gamma, \Delta)$  and  $\mathcal{L} = \mathcal{L}(\gamma, \Delta, \Gamma)$ . For  $H = 0$ , the dissipative term proportional to  $\Gamma$  would result in relaxation of the first spin into the fully polarized state in the  $z$  direction, namely  $|\uparrow\rangle\langle\uparrow|$ , where  $\sigma^z|\uparrow\rangle = |\uparrow\rangle$ , with a relaxation time of order  $1/\Gamma$ .

We will find the solution of Eq. (1) by solving the associated eigenvalue problem  $\mathcal{L}\rho = \lambda\rho$  in vector form [18]  $\text{vec}(\mathcal{L}\rho) = \mathcal{L}_{\text{vec}}\text{vec}(\rho) = \lambda\text{vec}(\rho)$ . The corresponding vectorized Liouvillian is given by the  $16 \times 16$  matrix

$$\begin{aligned} \mathcal{L}_{\text{vec}} = & -iH \otimes I_4 + iI_4 \otimes H^T \\ & + \Gamma (L \otimes L^\dagger - \frac{1}{2}(L^\dagger L) \otimes I_4 - \frac{1}{2}I_4 \otimes (L^\dagger L)^T). \end{aligned} \quad (4)$$

Both the Hamiltonian  $H$  and the Lindblad operator  $L$  commute with the operator  $\Sigma_z = \sigma^z \otimes \sigma^z$ , namely,

$$[\Sigma_z, H] = 0, \quad [\Sigma_z, L] = 0. \quad (5)$$

These relations can be used to block-diagonalize the vectorized Liouvillian  $\mathcal{L}_{\text{vec}}$  as follows. Introduce the matrices  $Q_\pm = \frac{1}{2}(I_{16} \pm \Sigma_z \otimes \Sigma_z)$  which satisfy

$$\begin{aligned} Q_+ + Q_- &= I_{16}, \\ [Q_\pm, \mathcal{L}_{\text{vec}}] &= 0, \\ Q_\pm Q_\mp &= 0, \quad Q_\pm \mathcal{L}_{\text{vec}} Q_\mp = 0. \end{aligned} \quad (6)$$

From these relations we have  $\mathcal{L}_{\text{vec}} = \mathcal{L}_+ + \mathcal{L}_-$ , where  $\mathcal{L}_\pm = Q_\pm \mathcal{L}_{\text{vec}} Q_\pm$  are matrices of rank 8 satisfying  $\mathcal{L}_\pm \mathcal{L}_\mp = 0$ . The block diagonalization of the vectorized Liouvillian is then achieved as

$$\mathcal{L}_{\text{vec}} = \Sigma_+ \oplus \Sigma_- = \begin{pmatrix} \Sigma_+ & 0 \\ 0 & \Sigma_- \end{pmatrix}, \quad (7)$$

where  $\Sigma_\pm$  are  $8 \times 8$  diagonal-blocks, obtained from  $\mathcal{L}_\mp = 0$  by eliminating the eight null rows and columns present in these matrices, see [19] for explicit matrix elements.

*Liouvillian spectrum and LEPs.*—The full Liouvillian spectrum can be obtained by diagonalizing the blocks  $\Sigma_\pm$  separately. Since the parameter  $\Delta$  appears only in the lower diagonal block  $\Sigma_-$  [19], the block diagonalization allows to separate the  $\Delta$ -dependent and  $\Delta$ -independent parts of the spectrum into two orthogonal spaces.

The secular equation for the eigenvalues of the block  $\Sigma_+$  is given by  $\lambda(\Gamma + \lambda)(\Gamma + 2\lambda)^2\Lambda(\gamma, \Gamma) = 0$ , where  $\Lambda(\gamma, \Gamma)$  is the quartic polynomial in  $\lambda$

$$\begin{aligned} \Lambda(\gamma, \Gamma) = & \lambda^4 + 2\Gamma\lambda^3 + \left[8(1 + \gamma^2) + \frac{5}{4}\Gamma^2\right]\lambda^2 \\ & + \left[8(1 + \gamma^2)\Gamma + \frac{\Gamma^3}{4}\right]\lambda \\ & + 2[8(1 + \gamma^4) + \Gamma^2 + \gamma^2(\Gamma^2 - 16)]. \end{aligned}$$

Thus, the eight  $\Delta$ -independent eigenvalues of  $\Sigma_+$  are

$$\begin{aligned} \lambda(\gamma, \Gamma) = & \left\{ 0, -\Gamma, -\frac{\Gamma}{2}, -\frac{\Gamma}{2}, -\frac{\Gamma}{2} \pm \frac{\sqrt{2}}{4} \right. \\ & \left. \times \sqrt{\Gamma^2 - 32(1 + \gamma^2) \pm \sqrt{(\Gamma^2 - 64)(\Gamma^2 - 64\gamma^2)}} \right\}. \end{aligned} \quad (8)$$

From Eq. (8) we see that these eigenvalues always have branching points at two different values of  $|\Gamma|$ , namely,  $|\Gamma| = 8$  and  $|\Gamma| = 8|\gamma|$ . No other singular points are found for  $\lambda(\gamma, \Gamma)$ .

The eight  $\Delta$ -dependent eigenvalues of the block  $\Sigma_-$  are given by, see [19] for details,

$$\lambda = \frac{1}{2} \left( -\Gamma \pm \sqrt{\Gamma^2 + \xi_i} \right), \quad i = 1, \dots, 4, \quad (9)$$

where  $\xi_i = \xi_i(\gamma, \Delta, \Gamma)$  are the roots of the quartic polynomial

$$c_a \xi^4 + c_b \xi^3 + c_c \xi^2 + c_d \xi + c_e = 0, \quad (10)$$

with coefficients  $c_a, c_b, c_c, c_d, c_e$  which depend on  $\gamma, \Delta, \Gamma$  and are detailed in [19]. Due to the complex nature of the eigenvalues of  $\mathcal{L}$ , it is clear that the argument of the square root in Eq. (9) cannot change sign giving rise to branching points. However, in the analytical expressions of  $\xi_1, \dots, \xi_4$  there appear the same following square root [19]  $(p_1^2 - 4(c_c^2 - 3c_b c_d + 12c_a c_e)^3)^{1/2}$ , where  $p_1 = 2c_c^3 - 9c_b c_c c_d + 27(c_a c_d^2 + c_b^2 c_e) - 72c_a c_c c_e$ , whose argument does change sign as a function of the parameters  $\gamma, \Delta, \Gamma$ . Analogously to Eq. (8), we thus find that the  $\Sigma_-$  eigenvalues have branching points for any real positive solution of the equation

$$p_1^2 - 4(c_c^2 - 3c_b c_d + 12c_a c_e)^3 = 0. \quad (11)$$

One can show that Eq. (11) is equivalent to the following eight degree polynomial equation in the  $Z = \Gamma^2$  variable

$$\sum_{i=0}^8 a_i(X, Y) Z^i = 0, \quad (12)$$

with coefficients  $a_i$  which are polynomials in  $Y = \Delta^2$  with coefficients which are polynomials in  $X = \gamma^2$  [19]. This nested polynomial structure reveals the complexity of the LEPs in the parameter space.

We stress that the equations determining the branching points of both the  $\Sigma_+$  and  $\Sigma_-$  eigenvalues depend on the squares of the parameters  $\gamma, \Delta, \Gamma$ . It follows that our results are invariant with respect to a change of sign of each one of these parameters. Hereafter, for simplicity, we will assume that  $\gamma, \Delta, \Gamma$  are all positive [20]. Depending on the values of the parameters  $\gamma$  and  $\Delta$ , we have LEPs, corresponding to branching points in  $\text{Re } \lambda(\Gamma)$  and  $\text{Im } \lambda(\Gamma)$  at up to  $2 + 6 = 8$  different values of  $\Gamma$ . An example with LEPs at 2+5 different values of  $\Gamma$  is shown in Fig. 2, other examples are given in [19].

In general, at an EP the eigenvalue coalescence goes along with an eigenvector coalescence [21], this means non diagonalizability of the Liouvillian at any LEP. In [19] we provide analytic expressions of the Liouvillian eigenvectors on various LEPs explicitly showing the characteristic Jordan block decomposition of  $\Sigma_{\pm}$ .

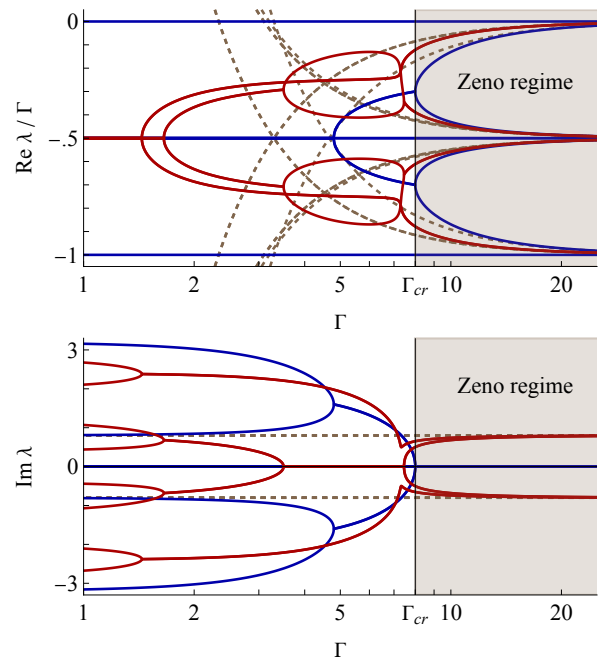


FIG. 2. Eigenvalues  $\lambda$  of the Liouvillian of the two-qubit open system (1) versus dissipation  $\Gamma$ . Top and bottom panels represent the real and imaginary parts of  $\lambda$ , in each panel, blue and red dots indicate the  $\Delta$ -independent and  $\Delta$ -dependent eigenvalues, respectively. Note the logarithmic horizontal scale. Parameters:  $\gamma = 0.6$ ,  $\Delta = 0.4$ , corresponding to the point labelled b in the right panel of Fig. 4. The LEPs coincide with the eigenvalue branching points. The dashed lines are the eigenvalues of  $\mathcal{L}$  evaluated in the near Zeno limit  $\Gamma \gg \Gamma_{cr}$ , where  $\Gamma_{cr}$  is the dissipation value beyond which all Liouvillian eigenvalues are analytical.

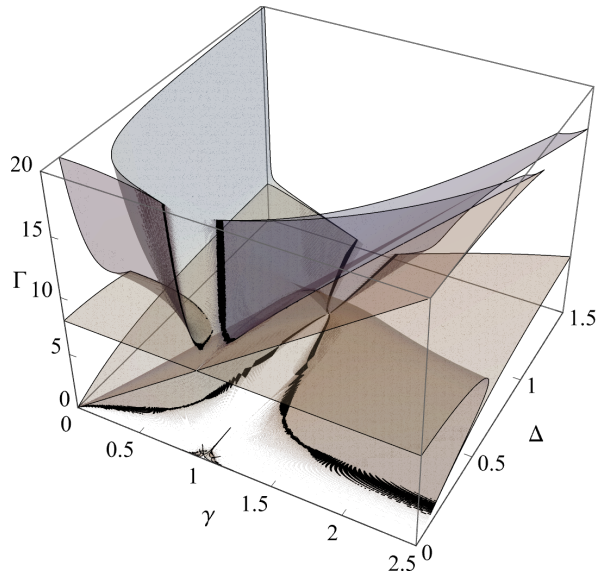


FIG. 3. Two-dimensional LEP manifolds of the two-qubit open system (1) in the three-dimensional parameter space  $\{\gamma, \Delta, \Gamma\}$ . Only the LEP manifolds originating from the  $\Delta$ -dependent block  $\Sigma_-$  of the Liouvillian are shown here.

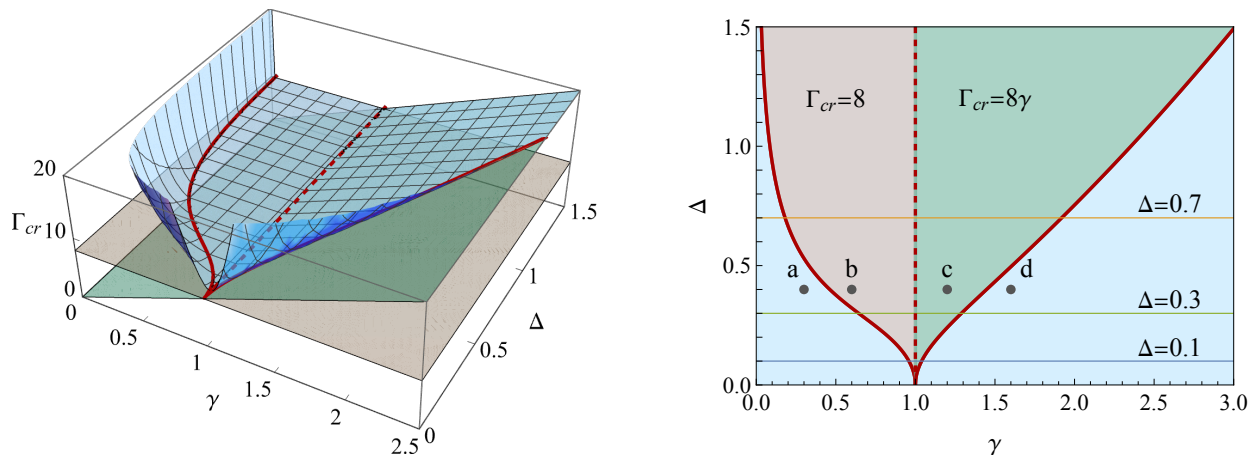


FIG. 4. Left panel. Behavior of  $\Gamma_{cr}(\gamma, \Delta)$ , light-blue surface with a mesh, for  $\Delta \geq 0.05$ . In the region delimited by the red continuous line this surface coincides with the straight planes  $\Gamma_{cr} = 8$  (displayed in gray) and  $\Gamma_{cr} = 8\gamma$  (displayed in green). Right panel. Two-dimensional diagram of  $\Gamma_{cr}(\gamma, \Delta)$ . The solid red line divides the plane  $\gamma, \Delta$  into two regions. Above this line we have  $\Gamma_{cr} = 8$  to the left of the  $\gamma = 1$  dashed line (gray region) and  $\Gamma_{cr} = 8\gamma$  to its right (green region). Note that the solid red line has a cusp  $\Delta = \frac{1}{2}\sqrt{|\gamma-1|}$  at the point  $(1, 0)$ . Below this line  $\Gamma_{cr}$  corresponds to a LEP arising from an eigenvalue of  $\Sigma_-$  and is an effective function of both  $\gamma, \Delta$ . In this region  $\Gamma_{cr}$  increases as  $\Delta$  is decreased, and diverges for  $\Delta \rightarrow 0$ , see Eq. (15). The same is true also for  $\gamma \rightarrow 0$ . On the  $\gamma = 1$  dashed red line,  $\Gamma_{cr}$  remains bounded to 8 for all values of  $\Delta$ , including  $\Delta = 0$ . The detailed branching point structure of the Liouvillian eigenvalues at the point labelled b is shown in Fig. 2. The same info at points a, c, and d is provided in [19]. In [19] we also show the sections of  $\Gamma_{cr}(\gamma, \Delta)$  at the planes  $\Delta = 0.1, 0.3$ , and  $0.7$  whose projections are indicated here by tiny solid lines.

In the three-dimensional space of parameters  $\gamma, \Delta, \Gamma$  the values of  $\Gamma$  for which LEPs are found form two-dimensional manifolds  $\Gamma(\gamma, \Delta)$ . The LEP manifolds originating from the  $\Delta$ -dependent block  $\Sigma_-$  of the Liouvillian is shown in Fig. 3. Due to the divergence of some manifolds in the limit  $\Delta \rightarrow 0$ , see later, the plot is limited to  $\Delta \geq 0.05$ . The two manifolds originating from the  $\Delta$ -independent block  $\Sigma_+$  of the Liouvillian, not shown in Fig. 3, correspond to the straight planes  $\Gamma = 8$  and  $\Gamma = 8|\gamma|$ .

Aiming at applications of Zeno limit results, we look at the location of the LEPs corresponding to the largest  $\Gamma$  value. Denoting by  $\Gamma_{LEP,j}$  the  $\Gamma$ -coordinates of the branching points occurring in the  $(\Gamma, \lambda_j)$  plane, see Fig 2, we define  $\Gamma_{cr}(\gamma, \Delta) = \sup_j \Gamma_{LEP,j}$ . The behavior of  $\Gamma_{cr}(\gamma, \Delta)$  is shown in Fig. 4, as a bare three-dimensional plot in the left panel and as a  $(\gamma, \Delta)$  diagram in the right panel. Remarkably, the plane  $\gamma, \Delta$  is divided in two regions by a boundary line given parametrically in [19]. The first region above the boundary line can be further divided in two parts: we have  $\Gamma_{cr} = 8$  for  $\gamma < 1$  and  $\Gamma_{cr} = 8\gamma$  for  $\gamma > 1$ . In the second region below the boundary line,  $\Gamma_{cr}$  corresponds to a LEP arising from an eigenvalue of  $\Sigma_-$  and is an effective function of both  $\gamma, \Delta$ . This function diverges for  $\Delta \rightarrow 0$  (with the exception of  $\gamma = 1$ ) and for  $\gamma \rightarrow 0$ .

The dynamical behavior of our system becomes fully analytic for  $\Gamma > \Gamma_{cr}$ , in fact, no singularities arise in this region. This makes it possible to write an expansion

in terms of  $1/\Gamma$ , which provides, as explained below, an effective near Zeno dynamics mechanism. It is therefore justified to say that for  $\Gamma > \Gamma_{cr}$  we enter a Zeno regime.

*Effective near Zeno dynamics.*—If the dissipation is strong, and in the absence of branching points, i.e., for  $\Gamma \gg \Gamma_{cr}$ , all Liouvillian eigenvalues can be calculated explicitly using a perturbative Dyson series [22]. For the present two-qubit open system the full set of 16 Liouvillian eigenvalues up to order  $1/\Gamma$  included is given by

$$\begin{aligned} \lambda_{0,\alpha} &= \left\{ 0, -2\frac{\gamma_+}{\Gamma}, -\frac{\gamma_+}{\Gamma} \pm 2\Delta i \right\}, \\ \lambda_{1,\alpha} &= \left\{ -\frac{\Gamma}{2}, -\frac{\Gamma}{2}, -\frac{\Gamma}{2} \pm \frac{2\gamma_-}{\Gamma}, -\frac{\Gamma}{2} \pm \frac{8\gamma}{\Gamma} \pm 2\Delta i \right\}, \\ \lambda_{2,\alpha} &= \left\{ -\Gamma, -\Gamma + 2\frac{\gamma_+}{\Gamma}, -\Gamma + \frac{\gamma_+}{\Gamma} \pm 2\Delta i \right\}, \end{aligned}$$

where  $\gamma_{\pm} = 4(1 \pm \gamma^2)$ . The eigenvalues are labeled by a stripe index, numbers 0,1,2, and a mode index, Greek letters  $\alpha$  ranging from 1 to 4 for stripes 0 and 2 and from 1 to 8 for stripe 1, see [22]. The modes  $\lambda_{0,\alpha}$  contain the nonequilibrium stationary state (NESS), corresponding to the null eigenvalue, and the slowest relaxation modes, which determine the late time evolution. On the other hand, the modes  $\lambda_{1,\alpha}, \lambda_{2,\alpha}$  have large negative real parts and thus correspond to rapid relaxation of the first spin towards the target state, namely, the qubit fully polarized along the  $z$ -axis.

The Liouvillian eigenvalues calculated in the near Zeno limit are shown in Fig. 2 by dashed lines. The theory



also predicts [22] explicit analytic expressions for the Liouvillian eigenvectors as well as an effective near Zeno dynamics. Namely, while the first spin relaxes towards the target state  $|\uparrow\rangle\langle\uparrow|$  in a time  $t = O(1/\Gamma)$ , the second spin has a slower dynamics described by a reduced effective Lindblad equation [23]. In fact, for  $t \gg 1/\Gamma$  up to an error  $O(1/\Gamma^2)$  we have  $\rho(t) = |\uparrow\rangle\langle\uparrow| \otimes R(t)$  with  $R(t)$  satisfying

$$\begin{aligned} \frac{\partial R}{\partial t} &= -i[h_D, R] + \frac{1}{\Gamma}(\tilde{L}R\tilde{L}^\dagger - \frac{1}{2}(\tilde{L}^\dagger\tilde{L}R + R\tilde{L}^\dagger\tilde{L})) \\ h_D &= \Delta\sigma^z, \\ \tilde{L} &= 4(\sigma^x + i\gamma\sigma^y). \end{aligned} \quad (13)$$

Note that for  $R(t)$  we have a dissipation strength  $1/\Gamma$  not  $\Gamma$  as in Eq. (1) for  $\rho(t)$ . The near Zeno limit NESS is found straightforwardly as the time independent solution of Eq. (13). This yields

$$\rho_{\text{Zeno}} = |\uparrow\rangle\langle\uparrow| \otimes \left( \begin{array}{cc} \frac{(\gamma+1)^2}{2(\gamma^2+1)} & 0 \\ 0 & \frac{(\gamma-1)^2}{2(\gamma^2+1)} \end{array} \right) + O\left(\frac{1}{\Gamma}\right). \quad (14)$$

In order to apply the Zeno limit predictions we must be sure that the  $1/\Gamma$  Dyson perturbative expansion is convergent. Since convergent series, which provide a unique sum, become invalid across branching points, we expect the  $1/\Gamma$  Taylor series of each Liouvillian eigenvalue  $\lambda_j$  to have a convergence radius  $1/\Gamma_{\text{LEP}}(\lambda_j)$ , where  $\Gamma_{\text{LEP}}(\lambda_j)$  is the largest  $\Gamma$  location of the branching points of  $\lambda_j$ , see Fig. 2. Beyond the point  $\Gamma_{cr}$  defined above *all* Liouvillian eigenvalues  $\lambda_j$  become analytical. On the  $\gamma, \Delta$  plane,  $\Gamma_{cr}$  is always finite, except in proximity of the lines  $\Delta = 0$  and  $\gamma = 0$  where a singularity arises. We find that  $\Gamma_{cr}(\Delta)$  for  $\Delta \rightarrow 0^+$  behaves as

$$\Gamma_{cr}(\Delta \rightarrow 0^+) = \max\left(\left|\frac{2(\gamma^2 - 1)}{\Delta}\right|, \left|\frac{\gamma^3 - 1/\gamma}{\Delta}\right|\right). \quad (15)$$

This singularity originates from the fact that at  $\Delta = 0$  the spectrum of the dissipation projected Hamiltonian  $h_D = \Delta\sigma^z$ , see Eq. (13), becomes degenerate.

*Conclusions.*—We have analytically investigated the Liouvillian spectrum of two qubit systems described by a Heisenberg chain with anisotropies  $\gamma$  and  $\Delta$  and dissipation of strength  $\Gamma$  applied to one qubit. We took advantage of a  $\mathcal{Z}_2$  symmetry to block-diagonalized the Liouvillian into two blocks, one of which independent of  $\Delta$ . This allowed us to derive polynomial equations that describe all LEPs of the system. We showed that for the  $\Delta$ -independent block, LEPs reduce to two planes, while for the other block, LEPs exhibit more intricate topologies with several sheets. We also identified the regions where the LEPs diverge relating this behavior to the presence of degeneracies in the spectrum of the system. Finally, we have provided a full analytic description of the temporal dynamics of the system in the

quantum Zeno regime. This regime becomes valid when the strength  $\Gamma$  of the dissipation acting on the system is much stronger than  $\Gamma_{cr}$ , namely the largest  $\Gamma$  coordinate among all the LEPs. We have identified all the regions where  $\Gamma_{cr}$  is small, and thus the effective Zeno regime is reached already for modest dissipation strengths. This makes Zeno behavior observable without employing strict (and usually very demanding) Zeno conditions.

We believe these results provide a detailed framework for understanding the interplay of dissipation and EPs in quantum systems, with implications for advancing quantum control, sensing, and computation.

V. P. acknowledges support by ERC Advanced grant No. 101096208 – QUEST, and Research Programme P1-0402 of Slovenian Research and Innovation Agency (ARIS), and from Deutsche Forschungsgemeinschaft through DFG project KL645/20-2.

- 
- [1] T. Kato, *A Short Introduction to Perturbation Theory for Linear Operators* (Springer-Verlag, New York 1982).
  - [2] W. D. Heiss, The physics of exceptional points, *J. Phys. A: Math. Theor.* **45**, 444016 (2012).
  - [3] M. A. Miri and A. Alù, Exceptional points in optics and photonics, *Science* **363**, eaar7709 (2019).
  - [4] J. Wiersig, Review of exceptional point-based sensors, *Photon. Res.* **8**, 1457 (2020).
  - [5] D. Anderson, M. Shah, and L. Fan, Clarification of the Exceptional-Point Contribution to Photonic Sensing, *Physical Review Applied*, **19**, 034059 (2023).
  - [6] M. Yang, L. Zhu, Q. Zhong, R. El-Ganainy, and P.-Y. Chen, Spectral sensitivity near exceptional points as a resource for hardware encryption, *Nature Comm.* **14**, 1145 (2023).
  - [7] J. W. Zhang et al, Dynamical control of quantum heat engines using exceptional points, *Nature Comm.* **13**, 6225 (2022).
  - [8] I. I. Arkhipov et al, Dynamically crossing diabolic points while encircling exceptional curves: A programmable symmetric-asymmetric multimode switch, *Nature Comm.* **14**, 2076 (2023).
  - [9] A. Li et al, Exceptional points and non-Hermitian photonics at the nanoscale, *Nature Nanotechnology* **18**, 706 (2023).
  - [10] G. Lindblad, On the generators of quantum dynamical semi-groups, *Commun. Math. Phys.* **48**, 119 (1976).
  - [11] V. Gorini, A. Kossakowski, and E. C. G. Sudarshan, Completely positive dynamical semigroups of N-level systems, *J. Math. Phys.* **17**, 821 (1976).
  - [12] H.-P. Breuer and F. Petruccione, *The Theory of Open Quantum Systems* (Oxford University Press, Oxford, 2002).
  - [13] F. Minganti, A. Miranowicz, R. W. Chhajlany, and F. Nori, Quantum exceptional points of non-Hermitian Hamiltonians and Liouvillians: The effects of quantum jumps, *Phys. Rev. A* **100**, 062131 (2019).
  - [14] J. Xu and Y. Guo, Unconventional steady states and topological phases in an open two-level non-Hermitian system, *New J. Phys.* **24**, 053028 (2022).

- [15] N. Seshadri, A. Li, and M. Galperin, Liouvillian exceptional points of an open driven two-level system, *J. Chem. Phys.* **160**, 044116 (2024).
- [16] Y.-L. Zhou et al, Accelerating relaxation through Liouvillian exceptional point, *Phys. Rev. Res.* **5** 043036 (2023).
- [17] M. Nakagawa, N. Kawakami, and M. Ueda, Exact Liouvillian spectrum of a one-dimensional dissipative Hubbard model, *Phys. Rev. Lett.* **126**, 110404.
- [18] Given the matrix  $A = [A_{ij}]_{i,j=1}^n$  we define the column vector  $\text{vec}(A) = (A_{11}, \dots, A_{1n}, \dots, A_{n1}, \dots, A_{nn})^T$ , where  $(\cdot)^T$  indicates matrix transpose. This implies  $\text{vec}(AB) = (A \otimes I_n)\text{vec}(B) = (B^T \otimes I_n)\text{vec}(A)$  and  $\text{vec}(ABC) = (A \otimes C^T)\text{vec}(B)$ , with  $A, B, C$  arbitrary matrices  $n \times n$ .
- [19] See Supplemental Material at . . . .
- [20] We restrict to real parameters to keep contact with realistic physical settings, however, LEPs exist for complex values of parameters as well.
- [21] K. Kanki, S. Garmon, S. Tanaka, and T. Petrosky, Exact description of coalescing eigenstates in open quantum systems in terms of microscopic Hamiltonian dynamics, *J. Math. Phys.* **58**, 092101 (2017).
- [22] V. Popkov and C. Presilla, Full Spectrum of the Liouvillian of Open Dissipative Quantum Systems in the Zeno Limit, *Phys. Rev. Lett.* **126**, 190402 (2021).
- [23] V. Popkov, S. Essink, C. Presilla, and G. Schütz, Effective quantum Zeno dynamics in dissipative quantum systems, *Phys. Rev. A* **98**, 052110 (2018).

# Supplemental Material: Manifolds of exceptional points and effective Zeno limit of an open two-qubit system

Vladislav Popkov,<sup>1,2</sup> Carlo Presilla,<sup>3,4</sup> and Mario Salerno<sup>5</sup>

<sup>1</sup>*Faculty of Mathematics and Physics, University of Ljubljana, Jadranska 19, SI-1000 Ljubljana, Slovenia*

<sup>2</sup>*Bergisches Universität Wuppertal, Gauss Str. 20, D-42097 Wuppertal, Germany*

<sup>3</sup>*Dipartimento di Matematica, Sapienza Università di Roma, Piazzale A. Moro 2, 00185 Rome, Italy*

<sup>4</sup>*Istituto Nazionale di Fisica Nucleare, Sezione di Roma 1, 00185 Rome, Italy*

<sup>5</sup>*Dipartimento di Fisica, Università di Salerno, Via Giovanni Paolo II, 84084 Fisciano (SA), Italy*

This Supplemental Material contains seven sections organized as follows. In section A we describe the block structure  $\Sigma_+, \Sigma_-$  of the Liouvillian. The polynomial equation whose roots provide the LEPs arising from  $\Sigma_-$  is detailed in section B. In section C we show some two-dimensional sections of the three-dimensional LEPs given in Fig. 3 as well as of  $\Gamma_{cr}(\gamma, \Delta)$  given in Fig. 4. The bifurcation diagrams at the four points indicated in Fig. 4 of the main text is shown in section D. In section E we make explicit the non-diagonalizability of the Liouvillian on the LEPs. Section F contains some subtle details regarding quantum Zeno regime which did not appear in the main text. Finally, in section G we explain how the boundary red line shown in Fig. 4 is obtained.

## A. Block diagonalization of the Liouvillian

The  $\mathcal{Z}_2$  symmetry discussed in the main text allows to put the Liouvillian in the form

$$\mathcal{L} = \begin{pmatrix} \Sigma_+ & 0 \\ 0 & \Sigma_- \end{pmatrix}, \quad (\text{S-1})$$

with the two  $8 \times 8$  diagonal-blocks,  $\Sigma_{\pm}$ , related to the  $\mathcal{Z}_2$  symmetry, achieved by eliminating the eight null rows and columns from the corresponding  $16 \times 16$  matrices  $\Sigma_{\pm} = \mathcal{U}_{\pm} \cdot \mathcal{L} \cdot \mathcal{U}_{\pm}$ . In Fig. S-1 we show the block structure of the Liouvillian  $\mathcal{L}$  obtained directly from Eq. (4) (left panel) and the one obtained after the  $\mathcal{Z}_2$  block diagonalization discussed in the main text (right panel).

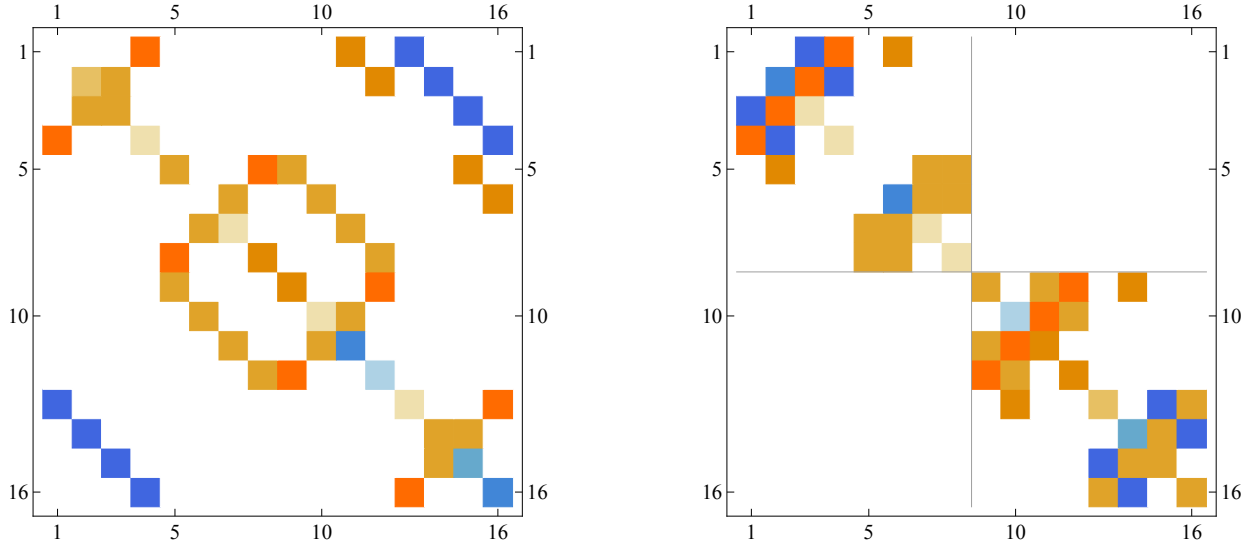


FIG. S-1. Liouvillian of the dissipative two qubit system as obtained from Eq. 4 (left panel) and its block diagonal form (right panel) acquired after operating the  $\mathcal{U}_{\pm}$  transformation. Colors are associated to different matrix elements, white regions corresponding to zeros (for other color correspondences see Eqs. S-3, S-4).

The blocks  $\Sigma_{\pm}$  can be further rearranged in the form

$$\Sigma_+ = \begin{pmatrix} A_1 & C \\ C & A_2 \end{pmatrix}, \quad \Sigma_- = \begin{pmatrix} B_1 & C \\ C & B_2 \end{pmatrix} \quad (\text{S-2})$$

with  $C$  a  $4 \times 4$  matrix whose single nonzero element is  $C_{1,2} = \Gamma$ , and  $A_1, A_2$  and  $B_1, B_2$  are given by:

$$A_1 = \begin{pmatrix} 0 & 0 & -i(1-\gamma) & i(1-\gamma) \\ 0 & -\Gamma & i(1-\gamma) & -i(1-\gamma) \\ -i(1-\gamma) & i(1-\gamma) & -\frac{\Gamma}{2} & 0 \\ i(1-\gamma) & -i(1-\gamma) & 0 & -\frac{\Gamma}{2} \end{pmatrix}, \quad (\text{S-3})$$

$$A_2 = \begin{pmatrix} 0 & 0 & i(\gamma+1) & -i(\gamma+1) \\ 0 & -\Gamma & -i(\gamma+1) & i(\gamma+1) \\ i(\gamma+1) & -i(\gamma+1) & -\frac{\Gamma}{2} & 0 \\ -i(\gamma+1) & i(\gamma+1) & 0 & -\frac{\Gamma}{2} \end{pmatrix},$$

$$B_1 = \begin{pmatrix} 2i\Delta & 0 & -i(\gamma+1) & i(1-\gamma) \\ 0 & -\Gamma + 2i\Delta & i(1-\gamma) & -i(\gamma+1) \\ -i(\gamma+1) & i(1-\gamma) & -\frac{\Gamma}{2} + 2i\Delta & 0 \\ i(1-\gamma) & -i(\gamma+1) & 0 & -\frac{\Gamma}{2} + 2i\Delta \end{pmatrix}, \quad (\text{S-4})$$

$$B_2 = \begin{pmatrix} -2i\Delta & 0 & -i(1-\gamma) & i(\gamma+1) \\ 0 & -\Gamma - 2i\Delta & i(\gamma+1) & -i(1-\gamma) \\ -i(1-\gamma) & i(\gamma+1) & -\frac{\Gamma}{2} - 2i\Delta & 0 \\ i(\gamma+1) & -i(1-\gamma) & 0 & -\frac{\Gamma}{2} - 2i\Delta \end{pmatrix}.$$

Note that the parameter  $\Delta$  appears only in the block  $\Sigma_-$ .

From the above expressions it is easy to find that the secular equation for the eigenvalues of the block  $\Sigma_+$  provides

$$\lambda(\Gamma + \lambda)(\Gamma + 2\lambda)^2 \Lambda(\gamma, \Gamma) = 0, \quad (\text{S-5})$$

where  $\Lambda(\gamma, \Gamma)$  is the quartic polynomial in  $\lambda$

$$\Lambda(\gamma, \Gamma) = \lambda^4 + 2\Gamma\lambda^3 + \left[8(1 + \gamma^2) + \frac{5}{4}\Gamma^2\right]\lambda^2 + \left[8(1 + \gamma^2)\Gamma + \frac{\Gamma^3}{4}\right]\lambda + 2[8(1 + \gamma^4) + \Gamma^2 + \gamma^2(\Gamma^2 - 16)]. \quad (\text{S-6})$$

We conclude that the eight  $\Delta$ -independent eigenvalues of  $\Sigma_+$  are

$$\lambda(\gamma, \Gamma) = \left\{ 0, -\Gamma, -\frac{\Gamma}{2}, -\frac{\Gamma}{2}, -\frac{\Gamma}{2} \pm \frac{\sqrt{2}}{4} \sqrt{\Gamma^2 - 32(1 + \gamma^2) \pm \sqrt{(\Gamma^2 - 64)(\Gamma^2 - 64\gamma^2)}} \right\}. \quad (\text{S-7})$$

On the other hand, the eight  $\Delta$ -dependent eigenvalues of the block  $\Sigma_-$  are given by

$$\lambda = \frac{1}{2} \left( -\Gamma \pm \sqrt{\Gamma^2 + \xi_i} \right), \quad i = 1, \dots, 4, \quad (\text{S-8})$$

where  $\xi_i = \xi_i(\gamma, \Delta, \Gamma)$  are the roots of the quartic polynomial  $c_a \xi^4 + c_b \xi^3 + c_c \xi^2 + c_d \xi + c_e = 0$  with coefficients

$$\begin{aligned} c_a &= 1, \\ c_b &= 2\Gamma^2 + 2^5(1 + \gamma^2) + 2^6\Delta^2, \\ c_c &= 2^5\Gamma^2(2(1 + \gamma^2) + 5\Delta^2) + \Gamma^4 + 2^8(2\gamma^4 + (1 + \gamma^2)^2 + 2(1 + \gamma^2)\Delta^2 + 6\Delta^4), \\ c_d &= 2^5(8\Gamma^2((1 + \gamma^2)^2 + 6\gamma^2 + 14\Delta^4) + \Gamma^4((1 + \gamma^2) + 5\Delta^2) \\ &\quad + 2^8(\gamma^2(1 + \gamma^2) + ((1 + \gamma^2)^2 - 6\gamma^2)\Delta^2 - (1 + \gamma^2)\Delta^4 + 2\Delta^6)), \\ c_e &= 2^6\Gamma^6\Delta^2 + 2^{16}(\gamma^2 - (1 + \gamma^2)\Delta^2 + \Delta^4)^2 + 2^8\Gamma^4(4\gamma^2 - 2(1 + \gamma^2)\Delta^2 + 9\Delta^4) \\ &\quad + 2^{12}\Gamma^2(2\gamma^2(1 + \gamma^2) + ((1 + \gamma^2) - 6\gamma^2)\Delta^2 - 4(1 + \gamma^2)\Delta^4 + 6\Delta^6). \end{aligned} \quad (\text{S-9})$$



By using Mathematica, we find

$$\begin{aligned}
\xi_1 &= -c_b/(4c_a) - p_4/2 - \sqrt{p_5 - p_6}/2, \\
\xi_2 &= -c_b/(4c_a) - p_4/2 + \sqrt{p_5 - p_6}/2, \\
\xi_3 &= -c_b/(4c_a) + p_4/2 - \sqrt{p_5 + p_6}/2, \\
\xi_4 &= -c_b/(4c_a) - p_4/2 + \sqrt{p_5 + p_6}/2,
\end{aligned} \tag{S-10}$$

where

$$\begin{aligned}
p_1 &= 2c_c^3 - 9c_b c_c c_d + 27c_a c_d^2 + 27c_b^2 c_e - 72c_a c_c c_e, \\
p_2 &= p_1 + \sqrt{p_1^2 - 4(c_c^2 - 3c_b c_d + 12c_a c_e)^3}, \\
p_3 &= (c_c^2 - 3c_b c_d + 12c_a c_e)/(3c_a \sqrt[3]{p_2/2}) + \sqrt[3]{p_2/2}/(3c_a), \\
p_4 &= \sqrt{c_b^2/(4c_a^2) - 2c_c/(3c_a)} + p_3, \\
p_5 &= c_b^2/(2c_a^2) - 4c_c/(3c_a) - p_3, \\
p_6 &= (-c_b^3/c_a^3 + 4c_b c_c/c_a^2 - 8c_d/c_a)/(4p_4).
\end{aligned} \tag{S-11}$$

Note that with  $\sqrt[3]{p_2/2}$  we mean the real-valued cube root of  $p_2/2$ .

### B. Polynomial equation for the LEP manifolds arising from $\Sigma_-$

In this section we show that all LEPs arising from  $\Sigma_-$  are obtained in the parameter space  $(\gamma, \Delta, \Gamma)$  as the roots of a polynomial of degree eight in the  $Z \equiv \Gamma^2$  variable, namely,

$$\sum_{i=0}^8 a_i(X, Y) Z^i = 0 \tag{S-12}$$

with coefficients  $a_i$  given by

$$\begin{aligned}
a_0 &= 2^{32}(X-1)^4 XY^2(X^2 + (1-4Y)^2 - 2X(1+4Y))^2, \\
a_1 &= -2^{27}(X-1)^8 XY + 2^{31}(X-1)^6 X(X+1)Y^2 + 2^{31}X(X-1)^4(1+30X+X^2)Y^3 \\
&\quad - 2^{35}(X-1)^2 X(X+1)(3+2X+3X^2)Y^4 + 2^{36}(X-1)^2 X(5+6X+5X^2)Y^5 - 2^{38}X(X-1)^2(X+1)Y^6, \\
a_2 &= 2^{20}(-1+X)^8 X + 2^{20}(-1+X)^6(1+X)(1-34X+X^2)Y - 2^{23}(-1+X)^4(1+24X+238X^2+24X^3+X^4)Y^2 \\
&\quad + 2^{24}(-1+X)^2(1+X)(1+44X-602X^2+44X^3+X^4)Y^3 + 2^{29}X(27+36X+2X^2+36X^3+27X^4)Y^4 \\
&\quad - 2^{33}X(1+X)(5-2X+5X^2)Y^5 + 2^{33}X(3+2X+3X^2)Y^6, \\
a_3 &= -2^{14}(-1+X)^6(1+X)(1-18X+X^2) + 2^{18}(-1+X)^4(1+4X+54X^2+4X^3+X^4)Y \\
&\quad + 2^{21}(1+X)(-1+X)^2(1+10X+42X^2+10X^3+X^4)Y^2 - 2^{20}(3+22X-883X^2-332X^3 \\
&\quad - 883X^4+22X^5+3X^6)Y^3 - 2^{26}X(1+X)(21+22X+21X^2)Y^4 + 2^{29}X(5+6X+5X^2)Y^5 - 2^{30}X(1+X)Y^6, \\
a_4 &= -256(-1+X)^4(15-60X-166X^2-60X^3+15X^4) - 2^{15}(-1+X)^2(1+X)(1+4X-42X^2+4X^3+X^4)Y \\
&\quad - 2^{16}(3+42X-3X^2-340X^3-3X^4+42X^5+3X^6)Y^2 + 2^{16}(1+X)(3-156X-974X^2-156X^3+3X^4)Y^3 \\
&\quad + 2^{21}X(39+74X+39X^2)Y^4 - 2^{24} * 5X(1+X)Y^5 + 2^24XY^6, \\
a_5 &= -64(3+X-21X^2+17X^3+17X^4-21X^5+X^6+3X^7) - 256(-1+X)^2(1+68X+246X^2+68X^3+X^4)Y \\
&\quad + 2^{13}(1+X)(1-6X+X^2)(1+14X+X^2)Y^2 - 2^{12}(1-236X-682X^2-236X^3+X^4)Y^3 - 2^{18} * 9X(1+X)Y^4 \\
&\quad + 2^{20}XY^5, \\
a_6 &= 4(1-2X-X^2+4X^3-X^4-2X^5+X^6) + 16(-1+X)^2(1+X)(5+38X+5X^2)Y \\
&\quad - 2^7(1-28X-138X^2-28X^3+X^4)Y^2 - 7 * 2^{12}X(1+X)Y^3 + 3 * 2^{13}XY^4, \\
a_7 &= -(1+4X-10X^2+4X^3+X^4)Y - 2^7X(1+X)Y^2 + 2^8XY^3,
\end{aligned}$$

$$a_8 = XY^2.$$

By inspection, one can readily check that Eq. (S-12) is equivalent to the condition (11) given in the main text. It is worth to note the multi polynomial structure of Eq. (S-12) having coefficients  $a_i$  which are polynomials in the variable  $Y \equiv \Delta^2$  with coefficients which, in turn, are polynomials in the variable  $X \equiv \gamma^2$ .

### C. Two-dimensional cuts of the LEP manifolds

In Fig. S-2 we show the two-dimensional sections at  $\Delta = 0.8$  (left panel) and  $\gamma = 1.5$  (right panel) of the three-dimensional LEP manifolds reported in Fig. 3. The solid blue lines are the sections of the  $\Delta$ -dependent LEPs arising from  $\Sigma_-$  while the dashed lines indicates the LEPs  $\Gamma = 8$  and  $\Gamma = 8\gamma$  from the  $\Delta$ -independent Liouvillian block  $\Sigma_+$ .

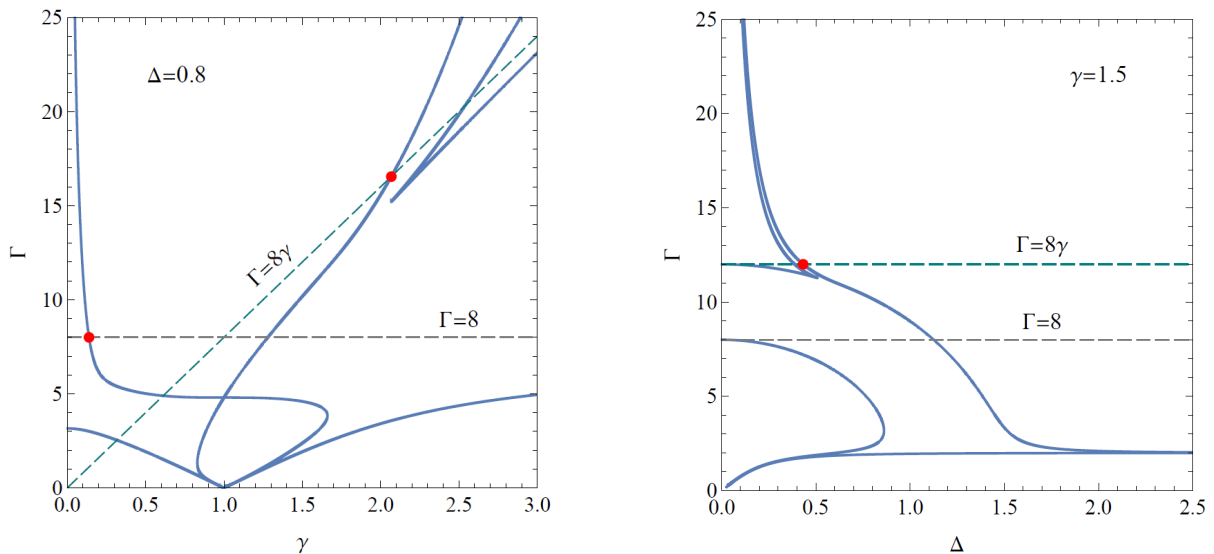


FIG. S-2. Two-dimensional sections at  $\Delta = 0.8$  (left panel) and  $\gamma = 1.5$  (right panel) of the manifolds shown in Fig. 3. The dashed straight lines indicate the intersections with the  $\Gamma = 8$  and  $\Gamma = 8\gamma$  planes (not shown in Fig. 3).

In Fig. S-3 we provide the two-dimensional sections at  $\Delta = 0.1, 0.3$ , and  $0.7$  of  $\Gamma_{cr}(\gamma, \Delta)$  given in Fig. 4. Also in this case, the dashed lines are the sections of the planes  $\Gamma = 8$  and  $\Gamma = 8\gamma$  which partially coincide with the  $\Delta$ -dependent sections shown by solid lines.

### D. Bifurcation diagrams at points a,b,c,d in Fig. 4 of the main text

In Fig. S-4 we depict the bifurcation diagrams obtained for the rescaled real part of all Liouvillian eigenvalues (from  $\Sigma_-$  as well as from  $\Sigma_+$ ) as a function of  $\Gamma$  for parameter values corresponding to points a, b, c, d of Fig. 4. In cases a,d the largest bifurcation belongs to the  $\Delta$ -dependent Liouvillian eigenvalues (red curves), while in cases b,c it belongs to the  $\Delta$ -independent Liouvillian eigenvalues (blue curves), in full agreement with the analysis done in the main text, see Fig. 4.

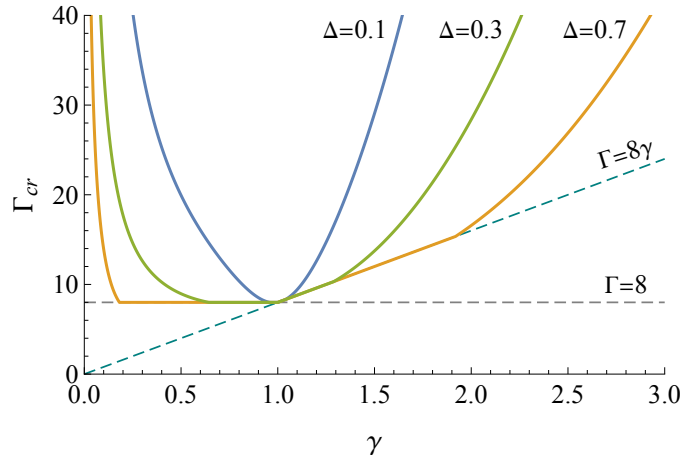


FIG. S-3. Two-dimensional sections at  $\Delta = 0.1, 0.3,$  and  $0.7$  of  $\Gamma_{cr}(\gamma, \Delta)$  of Fig. 4. The dashed lines are the sections of the planes  $\Gamma = 8$  and  $\Gamma = 8\gamma$ .

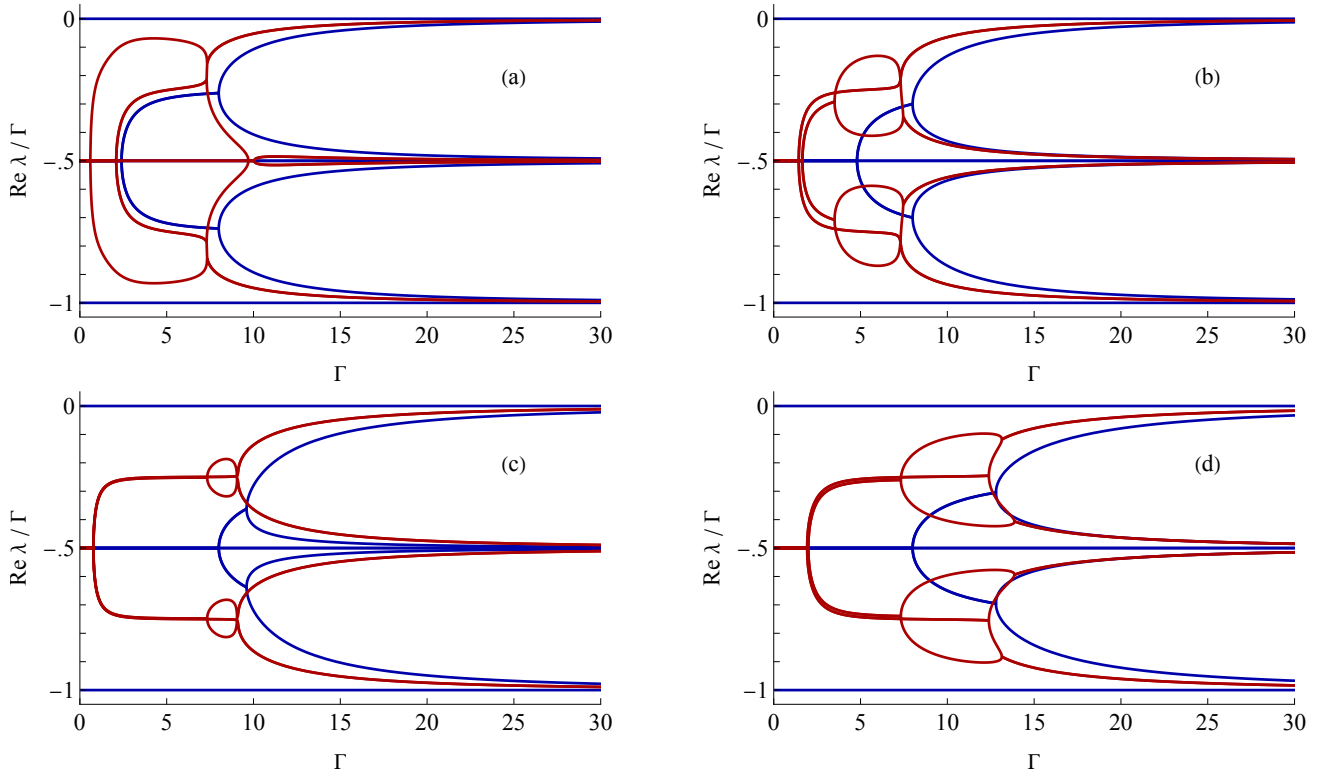


FIG. S-4. Rescaled real parts of the Liouvillian eigenvalues versus  $\Gamma$  for parameter values  $(\gamma, \Delta) = (0.3, 0.4), (0.6, 0.4), (1.2, 0.4),$  and  $(1.6, 0.4)$  corresponding, respectively, to the points a, b, c, and d depicted in Fig. 4 of the main text. Blue and red dots refer to  $\Delta$ -independent and  $\Delta$ -dependent eigenvalues, respectively. Notice that for the  $\Delta$ -independent part of the spectrum the first and second left most branching points occur at  $\Gamma = \min(8, 8\gamma)$  and at  $\Gamma = \max(8, 8\gamma)$ , respectively.

### E. Non-diagonalizability of the Liouvillian on LEPMs

In this section we show that on the LEPMs the Liouvillian matrix is non-diagonalizable. The analysis is made on the two diagonal blocks  $\Sigma_{\pm}$ , separately. For the block  $\Sigma_{+}$  the LEPMs are  $\Delta$  independent, they are the points of the two planes  $\Gamma = 8$  and  $\Gamma = 8\gamma$ . Eigenvalues and eigenvectors of  $\Sigma_{+}$  at these points are reported in Table I and II, respectively. In both cases, we note the presence of the null eigenvalue in the spectrum, meaning that the NESS of

-8	-4	-4	0	$2(-2 + \sqrt{1 - \gamma^2})$	$2(-2 + \sqrt{1 - \gamma^2})$	$-2(2 + \sqrt{1 - \gamma^2})$	$-2(2 + \sqrt{1 - \gamma^2})$
-1	0	0	$\frac{i(1+\gamma)(17-2\gamma+\gamma^2)}{4(-1+\gamma)^2}$	$-\frac{i(4+4\gamma+3\sqrt{1-\gamma^2}+\gamma\sqrt{1-\gamma^2})}{(1+\gamma)(2+\sqrt{1-\gamma^2})}$	0	$-\frac{i(-4-4\gamma+3\sqrt{1-\gamma^2}+\gamma\sqrt{1-\gamma^2})}{(1+\gamma)(-2+\sqrt{1-\gamma^2})}$	0
-1	0	0	$\frac{1}{4}i(1+\gamma)$	$\frac{i(-\sqrt{1-\gamma^2}+\gamma\sqrt{1-\gamma^2})}{(1+\gamma)(2+\sqrt{1-\gamma^2})}$	0	$\frac{i(-\sqrt{1-\gamma^2}+\gamma\sqrt{1-\gamma^2})}{(1+\gamma)(-2+\sqrt{1-\gamma^2})}$	0
0	0	1	$-\frac{1+\gamma}{-1+\gamma}$	$-\frac{1-\gamma}{\sqrt{1-\gamma^2}}$	0	$-\frac{-1+\gamma}{\sqrt{1-\gamma^2}}$	0
0	0	1	$-\frac{-1-\gamma}{-1+\gamma}$	$-\frac{-1+\gamma}{\sqrt{1-\gamma^2}}$	0	$-\frac{-1-\gamma}{\sqrt{1-\gamma^2}}$	0
1	0	0	$\frac{i(17+2\gamma+\gamma^2)}{4(1+\gamma)}$	$\frac{2i\sqrt{1-\gamma^2}}{1+\gamma} + \frac{i(1+\gamma)}{2+\sqrt{1-\gamma^2}}$	0	$\frac{i(-3-2\gamma+\gamma^2+4\sqrt{1-\gamma^2})}{(1+\gamma)(-2+\sqrt{1-\gamma^2})}$	0
1	0	0	$\frac{1}{4}i(1+\gamma)$	$\frac{i(1+\gamma)}{2+\sqrt{1-\gamma^2}}$	0	$-\frac{i(1+\gamma)}{-2+\sqrt{1-\gamma^2}}$	0
0	1	0	-1	-1	0	-1	0
0	1	0	1	1	0	1	0

TABLE I. Eigenvalues (top row) and eigenvectors (corresponding underlying columns) of the  $\Sigma_+$  diagonal block of the Liouvillian on the LEPM  $\{\gamma, \Delta, \Gamma = 8\}$ .

0	$-8\gamma$	$-4\gamma$	$-4\gamma$	$2(\sqrt{\gamma^2 - 1} - 2\gamma)$	$2(\sqrt{\gamma^2 - 1} - 2\gamma)$	$-2(\sqrt{\gamma^2 - 1} + 2\gamma)$	$-2(\sqrt{\gamma^2 - 1} + 2\gamma)$
$\frac{i(1+\gamma)(1-2\gamma+17\gamma^2)}{4(-1+\gamma)^2\gamma}$	-1	0	0	$-\frac{i(4\gamma+4\gamma^2+\sqrt{-1+\gamma^2}+3\gamma\sqrt{-1+\gamma^2})}{(1+\gamma)(2\gamma+\sqrt{-1+\gamma^2})}$	0	$-\frac{i(4\gamma+4\gamma^2-\sqrt{-1+\gamma^2}-3\gamma\sqrt{-1+\gamma^2})}{(1+\gamma)(2\gamma-\sqrt{-1+\gamma^2})}$	0
$\frac{i(1+\gamma)}{4\gamma}$	-1	0	0	$-\frac{i(-\sqrt{-1+\gamma^2}+\gamma\sqrt{-1+\gamma^2})}{(1+\gamma)(2\gamma+\sqrt{-1+\gamma^2})}$	0	$-\frac{i(-\sqrt{-1+\gamma^2}+\gamma\sqrt{-1+\gamma^2})}{(1+\gamma)(-2\gamma+\sqrt{-1+\gamma^2})}$	0
$-\frac{1+\gamma}{-1+\gamma}$	0	0	1	$-\frac{1-\gamma}{\sqrt{-1+\gamma^2}}$	0	$-\frac{-1+\gamma}{\sqrt{-1+\gamma^2}}$	0
$-\frac{-1-\gamma}{-1+\gamma}$	0	0	1	$-\frac{-1+\gamma}{\sqrt{-1+\gamma^2}}$	0	$-\frac{-1-\gamma}{\sqrt{-1+\gamma^2}}$	0
$\frac{i(1+2\gamma+17\gamma^2)}{4\gamma(1+\gamma)}$	1	0	0	$\frac{2i\sqrt{-1+\gamma^2}}{1+\gamma} + \frac{i(1+\gamma)}{2\gamma+\sqrt{-1+\gamma^2}}$	0	$-\frac{2i\sqrt{-1+\gamma^2}}{1+\gamma} - \frac{i(1+\gamma)}{-2\gamma+\sqrt{-1+\gamma^2}}$	0
$\frac{i(1+\gamma)}{4\gamma}$	1	0	0	$\frac{i(1+\gamma)}{2\gamma+\sqrt{-1+\gamma^2}}$	0	$-\frac{i(1+\gamma)}{-2\gamma+\sqrt{-1+\gamma^2}}$	0
-1	0	1	0	-1	0	-1	0
1	0	1	0	1	0	1	0

TABLE II. As in Table I on the LEPM  $\{\gamma, \Delta, \Gamma = 8\gamma\}$ .

the system, obtained from the corresponding eigenvector, belongs to the block  $\Sigma_+$ .

From Tables I and II it is evident that the coalescence of two pairs of complex eigenvalues (5th-6th and 7th-8th eigenvalues in both tables) is associated to the appearance of two null eigenvectors in the corresponding eigenspace. In fact, the dimension of the eigenspace is reduced as in the general case of linearly dependent eigenvectors. In other words, the  $\Sigma_+$  matrix becomes non-diagonalizable and its Jordan decomposition provides the typical Jordan blocks shown in Table III.

$$\Sigma_+(\gamma, \Delta, \Gamma = 8) = \begin{pmatrix} -8 & 0 & 0 & 0 & 0 & 0 & 0 & 0 \\ 0 & -4 & 0 & 0 & 0 & 0 & 0 & 0 \\ 0 & 0 & -4 & 0 & 0 & 0 & 0 & 0 \\ 0 & 0 & 0 & 0 & 0 & 0 & 0 & 0 \\ 0 & 0 & 0 & 0 & \alpha_+ & 1 & 0 & 0 \\ 0 & 0 & 0 & 0 & 0 & \alpha_+ & 0 & 0 \\ 0 & 0 & 0 & 0 & 0 & 0 & \alpha_- & 1 \\ 0 & 0 & 0 & 0 & 0 & 0 & 0 & \alpha_- \end{pmatrix} \quad \Sigma_+(\gamma, \Delta, \Gamma = 8\gamma) = \begin{pmatrix} 0 & 0 & 0 & 0 & 0 & 0 & 0 & 0 \\ 0 & -8\gamma & 0 & 0 & 0 & 0 & 0 & 0 \\ 0 & 0 & -4\gamma & 0 & 0 & 0 & 0 & 0 \\ 0 & 0 & 0 & -4\gamma & 0 & 0 & 0 & 0 \\ 0 & 0 & 0 & 0 & \beta_+ & 1 & 0 & 0 \\ 0 & 0 & 0 & 0 & 0 & \beta_+ & 0 & 0 \\ 0 & 0 & 0 & 0 & 0 & 0 & \beta_- & 1 \\ 0 & 0 & 0 & 0 & 0 & 0 & 0 & \beta_- \end{pmatrix}$$

TABLE III. Jordan block form of  $\Sigma_+$  on the LEPMs relative to Table I (left matrix) and Table II (right matrix). We put  $\alpha_{\pm} = -4 \pm 2\sqrt{1 - (8\gamma)^2}$  and  $\beta_{\pm} = -4\gamma \pm 2\sqrt{\gamma^2 - 1}$ .

$-6 - 2i\Delta$	$-6 - 2i\Delta$	$-2 - 2i\Delta$	$-2 - 2i\Delta$	$-6 + 2i\Delta$	$-6 + 2i\Delta$	$-2 + 2i\Delta$	$-2 + 2i\Delta$
$\frac{-2\Delta+i}{(\Delta+i)^2}$	0	0	0	0	0	$i$	0
0	0	0	0	$i(\Delta+i)^2$	0	0	0
$-\frac{1}{(\Delta+i)^2}$	0	0	0	0	0	1	0
0	0	0	0	$-i(\Delta+i)^2$	0	0	0
0	0	$-i$	0	$2\Delta+i$	0	0	0
$i$	0	0	0	0	0	0	0
1	0	0	0	0	0	0	0
0	0	1	0	1	0	0	0

TABLE IV. Eigenvalues and eigenvectors of the diagonal block  $\Sigma_-$ , arranged as in Table I, on the EP line  $\{\gamma = 1, \Delta, \Gamma = 8\}$ .

$$\Sigma_-(\gamma = 1, \Delta, \Gamma = 8) = \begin{pmatrix} \begin{array}{cc|cc|cc|cc} -8-2i & 1 & 0 & 0 & 0 & 0 & 0 & 0 \\ 0 & -8-2i & 0 & 0 & 0 & 0 & 0 & 0 \\ \hline 0 & 0 & -6+2i & 1 & 0 & 0 & 0 & 0 \\ 0 & 0 & 0 & -6+2i & 0 & 0 & 0 & 0 \\ \hline 0 & 0 & 0 & 0 & -4-2i & 1 & 0 & 0 \\ 0 & 0 & 0 & 0 & 0 & -4-2i & 0 & 0 \\ \hline 0 & 0 & 0 & 0 & 0 & 0 & -2+2i & 1 \\ 0 & 0 & 0 & 0 & 0 & 0 & 0 & -2+2i \end{array} \end{pmatrix}$$

TABLE V. Jordan block form of  $\Sigma_-$  on the LEPMs  $\{\gamma = 1, \Delta, \Gamma = 8\}$ .

Similar results are obtained for the  $\Sigma_-$  block of the Liouvillian. However, in the case of this  $\Delta$ -dependent block the LEPMs are much more involved with complicated topology and several sheets. Taking only positive real values for  $\gamma, \Delta$  and restricting to only real positive solutions of the polynomial equation (S-12), one can show that LEPM can have a number of sheets (branches) that varies from 1 to 6 depending on the values of  $\gamma, \Delta$ .

Analytical expressions for the Jordan block decomposition of  $\Sigma_-$ , except for a few simple cases (see below), are impossible to derive and one must recourse to numerical calculations. Using numerical solutions of Eq. (S-12) one finds for generic points on a LEPM, results qualitatively similar to those obtained for the block  $\Sigma_+$  with the difference that the NESS does not belong to the manifold and the number of pairs of complex coalescing eigenvalues can be maximal, i.e., as large as 4, depending on  $\gamma, \Delta$  values.

A particularly simple case in which the coalescence of the eigenvalues and eigenvectors of the  $\Sigma_-$  block can be checked analytically is obtained for  $\gamma = 1$ . In this case the coefficients of the polynomial appearing in Eq. (S-12) drastically simplify and it admits the real positive root  $\Gamma = 8$  for all values of  $\Delta$ . The corresponding LEPM then becomes the EP line  $\{\gamma = 1, \Delta, \Gamma = 8\}$ . Eigenvalues and eigenvectors of the  $\Sigma_-$  block along this line are reported in Table IV and the corresponding Jordan block decomposition is given in Table V.

## F. Convergence to NESS and characteristic dissipation value $\Gamma_{ch}$

The exact NESS of the two-qubit problem (when it is unique) can be evaluated analytically and is given by

$$\rho_{\text{NESS}}(\Gamma) = \begin{pmatrix} \frac{(\gamma+1)^2(4\gamma^2-8\gamma+\Gamma^2+4)}{2(8\gamma^4+\gamma^2(\Gamma^2-16)+\Gamma^2+8)} & 0 & 0 & -\frac{i(\gamma-1)(\gamma+1)^2\Gamma}{8\gamma^4+\gamma^2(\Gamma^2-16)+\Gamma^2+8} \\ 0 & \frac{(\gamma-1)^2(4\gamma^2+8\gamma+\Gamma^2+4)}{2(8\gamma^4+\gamma^2(\Gamma^2-16)+\Gamma^2+8)} & \frac{i(\gamma-1)^2(\gamma+1)\Gamma}{8\gamma^4+\gamma^2(\Gamma^2-16)+\Gamma^2+8} & 0 \\ 0 & \frac{i(\gamma-1)^2(\gamma+1)\Gamma}{-8\gamma^4+\gamma^2(\Gamma^2-16)+\Gamma^2+8} & \frac{2(\gamma-1)^2(\gamma+1)^2}{8\gamma^4+\gamma^2(\Gamma^2-16)+\Gamma^2+8} & 0 \\ \frac{i(\gamma-1)(\gamma+1)^2\Gamma}{8\gamma^4+\gamma^2(\Gamma^2-16)+\Gamma^2+8} & 0 & 0 & \frac{2(\gamma-1)^2(\gamma+1)^2}{8\gamma^4+\gamma^2(\Gamma^2-16)+\Gamma^2+8} \end{pmatrix}. \quad (\text{S-13})$$

Note that the NESS is  $\Delta$ -independent. In the quantum Zeno limit we have

$$\rho_{\text{Zeno}} = \lim_{\Gamma \rightarrow \infty} \rho_{\text{NESS}}(\Gamma) = |\uparrow\rangle \langle \uparrow| \otimes \begin{pmatrix} \frac{(\gamma+1)^2}{2(\gamma^2+1)} & 0 \\ 0 & \frac{(\gamma-1)^2}{2(\gamma^2+1)} \end{pmatrix}, \quad (\text{S-14})$$

in accordance with Eq. (14) obtained in the main text with the help of the reduced Zeno dynamics [23]. We observe that for large  $\Gamma$

$$\text{tr}(\rho_{\text{Zeno}}^2) - \text{tr}(\rho_{\text{NESS}}^2(\Gamma)) = O\left(\frac{1}{\Gamma^2}\right) + \dots \quad (\text{S-15})$$

so that this quantity can serve as a measure of the distance to the Zeno NESS for fixed values of the dissipation  $\Gamma$ .

Using Eq. (S-15) we introduce a characteristic dissipation strength  $\Gamma_{ch}$  needed to reach the Zeno NESS, as

$$\Gamma_{ch}^2(\gamma) = \lim_{\Gamma \rightarrow \infty} \Gamma^2 [\text{tr}(\rho_{\text{Zeno}}^2) - \text{tr}(\rho_{\text{NESS}}^2(\Gamma))] = \frac{4\gamma^{10} + 36\gamma^8 - 40\gamma^6 - 40\gamma^4 + 36\gamma^2 + 4}{\gamma^8 + 4\gamma^6 + 6\gamma^4 + 4\gamma^2 + 1}. \quad (\text{S-16})$$

First of all, note that  $\Gamma_{ch}$  is independent of  $\Delta$  and also it does not have any singularities for  $\gamma \rightarrow 0$ . This might seem in contradiction to what is stated in Eq. (15). To resolve the issue, we remark that the effective dynamics (13) only concerns the relaxation of the diagonal elements of the reduced density matrix, i.e., those elements which in the limit  $\Gamma \rightarrow \infty$  become the NESS eigenvalues. Expression (S-16) thus gives an estimate of the relaxation of a part of the system only, while for the relaxation of the non-diagonal part of the reduced density matrix  $\rho$  the full system (1) still needs to be considered.

### G. Obtaining the boundary lines in Fig. 4

Here we explain how we obtain the red boundary lines, shown in both panels of Fig. 4, separating the regions where  $\Gamma_{cr}$  corresponds to a LEP arising from an eigenvalue of  $\Sigma_+$  or  $\Sigma_-$ .

For the location of the left curve, we solve numerically Eq. (11) for  $\Delta$  fixing the value of  $\Gamma = 8$  and varying  $\gamma$  in the interval  $0 < \gamma < 1$ . This yields two branches of solutions  $\Delta_{1L}(\gamma) > 0$  and  $\Delta_{2L}(\gamma) > \Delta_{1L}(\gamma)$ . The upper branch  $\Delta_{2L}(\gamma)$  gives the red line in Fig. 4 in the interval  $0 < \gamma < 1$ .

Likewise, in the region  $1 < \gamma$  we solve Eq. (11) for  $\Delta$ , fixing the value of  $\Gamma = 8\gamma$  and varying  $\gamma > 1$ . Also in this case we obtain two branches of solutions  $\Delta_{1R}(\gamma) > 0$  and  $\Delta_{2R}(\gamma) > \Delta_{1R}(\gamma)$ . The upper branch  $\Delta_{2R}(\gamma)$  gives the red line in Fig. 4 in the region  $\gamma > 1$ .